



Preliminary survey of matrix effects in the Microwave-sustained, Inductively Coupled Atmospheric-pressure Plasma (MICAP)

Klemens M. Thaler^{a,b}, Andrew J. Schwartz^{a,1}, Christoph Haisch^b, Reinhard Niessner^b, Gary M. Hieftje^{a,*}

^a Laboratory for Spectrochemistry, Indiana University, Bloomington, IN 47405, USA

^b Analytical Chemistry, Institute of Hydrochemistry, Technische Universität München, Marchioninistrasse 17, 81377 Munich, Germany

ARTICLE INFO

Keywords:

Elemental analysis
Atomic emission spectrometry
Matrix
Interferences
Nitrogen plasma

ABSTRACT

Matrix effects caused by Na and Al in the nitrogen Microwave-sustained, Inductively Coupled, Atmospheric-pressure Plasma (MICAP) were investigated. Easily ionizable elements, such as Na, can suppress or enhance the analyte signal; Al is shown here to produce a similar effect. The influence of these matrices was examined for 18 emission lines of 8 analyte atoms and ions having a wide range of excitation and ionization energies. The plasma operating conditions were fixed during all experiments at a total nitrogen flow of 19.4 L min⁻¹ and a microwave power of 1.5 kW. An Fe solution was used to determine the excitation temperature of the plasma by the Boltzmann plot method at selected matrix concentrations. In addition, vertical emission profiles of the plasma were measured. The matrix effect becomes worse at higher concentrations of an easily ionizable element. The effect is caused not only by a shift in ionization equilibrium but also by a possible change in plasma ionization temperature. Correction methods to reduce the matrix effects were tested and are discussed.

1. Introduction

Plasma sources for trace element analysis were introduced more than 50 years ago and have found widespread use for atomic emission spectrometry (AES) and as ionization sources for atomic mass spectrometry (MS) [1]. The inductively coupled plasma (ICP) is the most popular such plasma source and can achieve detection limits below ng/L, when combined with MS [2]. Detection limits for ICP-AES are usually higher; however, the possibility of using alternative emission lines of an analyte atom makes it possible to detect some elements (e.g. fluorine) that cannot readily be measured by ICP-MS [3]. Moreover, in ICP-MS, some isotopes suffer spectral interference; examples include ⁴⁰Ca which overlaps with ⁴⁰Ar, or ⁵⁶Fe, compromised by ⁴⁰Ar¹⁶O⁺ [4,5]. Quantification of these elements by ICP-MS requires the use of additional equipment such as collision cells or high mass resolution sector-field mass spectrometers [6,7].

Both ICP-AES and ICP-MS require substantial flows of the plasma-support gas (Ar), which leads to high operating costs. Accordingly, plasma sources employing alternative gases have been developed throughout the last decades and have received considerable attention [8–15]. Microwave-induced plasmas (MIPs) have been explored by many workers; however, most early MIP setups were operated at

200–300 W (up to 500 W), which provides insufficient plasma energy for efficient desolvation, vaporization and dissociation of aerosol droplets [9,16–18]. Later, high-power MIPs were developed that could determine some elements not easily measured by Ar-ICP-MS or Ar-ICP-AES [19,20]. For example, Pb detection limits in MIPs are usually better than for ICP-AES [21,22]. Also, for some special applications such as the sizing and elemental analysis of microparticles, MIP-AES was found to be more useful than ICP-AES [23,24].

Matrix effects are a continuing problem in atomic emission spectrometry. Generally, such effects are much more severe in MIPs than in the Ar-ICP [25]. For both ICP and MIP, several studies investigated the influence of easily ionized elements (EIEs) on analyte signals [26–28]. Elements such as Na, Ca, K or Li can cause suppression or enhancement of analyte signals and therefore hamper quantification of samples. The influence of EIEs on emission response is a matter of significant practical relevance and has to be examined before any new method for plasma generation can be used routinely for analytical applications. The influence of EIEs on the Microwave-sustained, Inductively Coupled Atmospheric-pressure Plasma (MICAP) has not been reported so far. In the present work, we describe the effect of Na on 18 emission lines of 8 analyte elements in the nitrogen MICAP. The effect of Al on the emission lines is compared to that of Na. Vertical profiles of emission

* Corresponding author.

E-mail address: hieftje@indiana.edu (G.M. Hieftje).

¹ Current address: State University of New York at Buffalo, 407 Natural Sciences Complex Buffalo, NY 14260-3000, USA.

intensity have been measured to study the effect of Na on the spatial intensity distribution. Additionally, excitation temperatures were determined by the Boltzmann plot method by using iron emission lines [29]. A comparison with matrix effects in other microwave-sustained nitrogen discharges is provided and methods to overcome matrix effects are considered.

2. Experimental

The MICAP setup employed throughout this study is similar to that described earlier [30]. A 1.5 kW magnetron was used to generate a microwave field that was directed into the resonator chamber by means of an aluminum waveguide. Within the chamber, two alternative Meinhard (Golden, CO) Leeman-type quartz ICP torches (ML155020 and ML155023) with a 1.5 mm or 2.5 mm inner diameter (i.d.) injector, respectively, and 18 mm i. d. outer tube were installed vertically. Most results shown here were measured with the torch having a 1.5 mm i.d. injector. For experiments to overcome the matrix effect, the 2.5 mm i.d. injector was used. Three gas streams of nitrogen were provided to the torch, with flows of 18, 0.4 and 1 L min⁻¹ for the outer, intermediate and central channels, respectively, except where noted otherwise. The gas streams were regulated by mass flow controllers. The outer-channel flow controller was a model GR116-10 from Fathom Technologies (Georgetown, TX), while the intermediate and inner-channel controllers were model AW9411059 from Tylan General (San Diego, CA). To ignite the MICAP, nitrogen was provided only to the outer channel, while microwave power (1.5 kW) was applied to the waveguide and resonator. At the same time, an argon flow (2 L min⁻¹) was briefly (~2 s) introduced into the intermediate channel, while a Tesla coil generated a spark within the gas line. After plasma ignition, the argon flow was turned off and the intermediate-channel and central-channel nitrogen flows initiated. Support gases consisted of industrial grade nitrogen ($\geq 99.998\%$ purity) and ultra-high purity argon ($\geq 99.999\%$), all supplied by Airgas (Radnor Township, PA). Sample solutions were introduced into the plasma by a Glass Expansion concentric nebulizer (model AR30-1-UC2TLL, Pocasset, MA) in conjunction with a single-pass cyclonic spray chamber (Meinhard, model C18303). Sample solutions were fed at a rate of 1 mL min⁻¹ by a Gilson (Middletown, WI) Miniplus 3 peristaltic pump. After introduction of each sample solution, the tubing was flushed with blank solution to prevent contamination and carryover.

All sample solutions were prepared in dilute (0.1 M) nitric acid, obtained from concentrated reagent-grade stock, purified in-house with a sub-boiling polytetrafluoroethylene distillation unit, and deionized water of 18.2 M Ω cm⁻¹ specific resistance. Primary analyte stock solutions (1000 mg L⁻¹ concentration) were obtained from High-Purity Standards (Charleston, SC) or prepared from analytical reagent-grade (or better) nitrate salts and dissolved in 0.1 M nitric acid. Samples of lower concentration were obtained by serial dilution (in 0.1 M nitric acid) of the primary stock standards. To investigate matrix effects, sodium or aluminum solutions (as NaNO₃ or AlCl₃·6H₂O, dissolved in 0.1 M nitric acid) were added to the analyte solutions. Concentrations of 25, 75 and 200 mM (0.58, 1.73 and 4.60 g L⁻¹) of Na and 25 mM (0.68 g L⁻¹) of Al were chosen.

Radiation from the MICAP was imaged by a plano-convex quartz lens (100-mm focal length, 50-mm diameter) with a magnification of 0.3 onto the 7-mm high, 10- μ m wide entrance slit of a 0.64 m Czerny-Turner spectrograph (model ACTIVA-M, Horiba Jobin-Yvon, Longjumeau, France) outfitted with two gratings. The first grating was used over the wavelength range of 120–430 nm, had a groove density of 4343 grooves mm⁻¹ and was used for the collection of spectral data from 200 to 430 nm. The second grating (2400 grooves mm⁻¹) was used for the collection of data from 430 to 800 nm. In order to match the numerical aperture of the quartz lens ($f/2$) to that of the spectrograph ($f/8.5$), an iris was placed immediately behind the lens, reducing the beam diameter to approximately 12 mm. Throughout all

experiments, the MICAP was viewed radially, and the observation zone covered 15–36 mm above the alumina resonator.

A two-dimensional, back-illuminated CCD detector (Andor, Belfast, Ireland, model DU-440-BU2-380), Peltier cooled to -38°C , was coupled to the spectrometer for detection. In this configuration, the CCD provides a two-dimensional image, with wavelength displayed on the horizontal axis, and vertical position in the plasma shown vertically. For all experiments, the camera was operated with a readout rate of 1 MHz; a 10-s integration (or its equivalent in summed exposures) was used. In each case, three images were collected for every measurement from the CCD by using the manufacturer software bundled with the ACTIVA-M spectrograph (ACTIVAnalyst v5.4.2). These images were subsequently processed offline with custom-programmed National Instruments (Austin, TX) LabVIEW® software or Matlab® (The MathWorks, Inc., Natick, MA).

Spatially resolved emission patterns of the investigated analyte species were measured in the presence as well as in the absence of the chosen interfering matrix. To obtain a vertical spatial profile of a particular emission line, 10–30 pixels (depending on the intensity of the emission line) around the center of the line were averaged horizontally (across the wavelength axis). The vertically resolved plots show these wavelength-averaged values, with zero on the spatial axis representing the upper edge of the MICAP ceramic resonator.

Spectra were extracted from the CCD images by vertically binning all pixels along the columns of the camera (i.e. across the vertical image of the MICAP), thereby summing emission intensity from 15 to 36 mm above the MICAP resonator, and thus representing column averages through an extended zone of plasma. Background spectra were collected from the nitric acid or blank matrix solution; all spectra shown here are background-subtracted. The reported values for analyte signal from these spectra are peak areas, integrated along the wavelength axis. The relative emission intensity was calculated as emission signal of a chosen spectral line in the presence of a matrix divided by the value in the absence of the matrix, at the concentration listed in Table 1. Values of relative emission intensity above one indicate that emission of the selected spectral line is enhanced by the matrix, whereas values below one represent signal suppression.

3. Results

3.1. Effect of sodium and aluminum on analytical signals

Addition of an EIE to a sample solution can cause either suppression or enhancement of MICAP emission lines, depending mainly on whether the lines arise from an analyte neutral atom or ion. An example is given in Fig. 1 for 1 $\mu\text{g mL}^{-1}$ Mg in 0.1 M HNO₃. Upon addition of 75 mM Na, the Mg II 279.55 nm and Mg II 280.27 nm ion lines are suppressed, while the atomic Mg I 285.21 nm line is enhanced. This trend of suppression of ionic emission and enhancement of atomic emission suggests that the effect involves a simple shift in ionization equilibrium [31–33].

Table 1 shows the effect of 25, 75 and 200 mM Na on 18 spectral lines of the analyte elements investigated in this study. Fig. 2 summarizes the relative emission intensities separately for ionic lines and atomic lines. For all ionic lines and at all Na matrix concentrations, suppression (values below 1.0) that increases with sodium concentration is observed. The presence of sodium at concentrations of 75 mM and above results in enhancement for all neutral-atom lines of Rb I, K I, Li I, Re I, and Mg I. The threshold energy sum (excitation plus ionization energy) for transitions to be either enhanced or suppressed was found to be between 4.4 eV and 7.7 eV. At lower sodium concentrations, the threshold for enhancement of emission lines shifts to lower excitation energies. Similar trends have been observed for a high power N₂-MIP sustained with an Okamoto cavity, where the effect was explained by a shift in atom/ion equilibrium [27].

Table 1 shows also the effect of 25 mM aluminum on the relative

Table 1

Relative emission intensities of selected spectral lines in the presence of either Na or Al matrices and Na concentrations, displayed in order of increasing excitation energy for atomic lines and energy sum (excitation + ionization energy) for ionic lines. Emission signals have been normalized to unity in the absence of a matrix.

Element and state	Wavelength/nm	Element concentration/ $\mu\text{g mL}^{-1}$	Excitation Energy/eV	Ionization Energy/eV	Sum/eV	Relative emission intensity in selected matrix			
						25 mM Na	75 mM Na	200 mM Na	25 mM Al
Rb I	780.027	10	1.59		1.59	1.25	2.12	3.25	1.36
K I	769.897	10	1.61		1.61	1.37	2.29	3.11	1.38
K I	766.490	10	1.62		1.62	1.33	2.29	2.97	1.35
Li I	670.791	1	1.85		1.85	1.17	2.26	3.34	1.48
Re I	346.046	10	3.60		3.60	0.89	1.33	1.55	1.22
Mg I	285.213	1	4.35		4.35	0.92	1.17	1.81	1.30
Ba II	493.408	1	2.51	5.21	7.72	0.81	0.79	0.70	0.90
Ba II	614.171	1	2.72	5.21	7.93	0.83	0.83	0.70	0.91
Ba II	455.403	1	2.72	5.21	7.93	0.63	0.61	0.52	0.96
Sr II	421.552	0.1	2.94	5.69	8.63	0.85	0.77	0.67	1.06
Sr II	407.771	0.1	3.04	5.69	8.73	0.87	0.84	0.72	1.09
Re II	221.426	10	n.a.	7.83	~ 11	0.70	0.80	0.55	0.74
Re II	227.525	10	n.a.	7.83	~ 11	0.79	0.77	0.53	0.84
Mg II	280.270	1	4.42	7.65	12.07	0.81	0.65	0.56	0.99
Mg II	279.553	1	4.43	7.65	12.08	0.81	0.65	0.57	1.00
Fe II	259.940	10	4.770	7.87	12.64	0.87	0.78	0.52	0.96
Fe II	259.837	10	4.818	7.87	12.69	0.89	0.81	0.52	0.96
Fe II	238.204	10	5.200	7.87	13.07	0.87	0.79	0.52	1.02

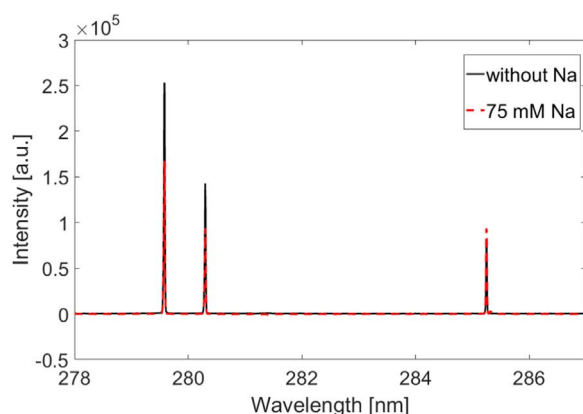


Fig. 1. Emission spectrum of $1 \mu\text{g mL}^{-1}$ Mg in 0.1 M HNO_3 without matrix (black line) and with 1.73 g L^{-1} (75 mM) Na (red line). Displayed emission lines are Mg II 279.55 nm, Mg II 280.27 nm and Mg I 285.21 nm. (For interpretation of the references to color in this figure legend, the reader is referred to the web version of this article.)

emission intensities of the same spectral lines. Again, neutral analyte-atom signals rise and ion signals drop when Al is present. Because the ionization energy of Al (5.9858 eV) is higher than that of Na (5.1391 eV) [34], Al would be expected to contribute somewhat less to interferences that result from a shift in ionization equilibrium.

3.2. Mg II/Mg I line-intensity ratio

In argon ICP-AES, the intensity ratio of the Mg II 280.27 nm and Mg I 285.21 nm lines is often used to assess the robustness of the plasma [35]; values larger than 10 indicate a robust plasma, one relatively immune to matrix interference [36]. The threshold value for this commonly used criterion is related to the electron number density in the discharge and has been applied most appropriately to the Ar-ICP. Values for microwave-induced nitrogen plasmas are lower because of the reduced electron number densities [37,38].

Matrix-dependent Mg II 280.27 nm/Mg I 285.21 nm ratios have been determined for the nitrogen MICAP and are displayed in Fig. 3. The highest values, observed in the absence of the Na matrix, are 1.8–1.9. These values are very low compared to those in an ICP, but similar to those in N_2 -MIPs sustained in a resonant-iris system (0.26 and 2.01) [25] and in an Okamoto cavity (0.5–2.5) [27]. At progressively higher Na concentrations, the Mg II/Mg I ratio in the MICAP shows an exponential decline. This behavior suggests that the matrix effect is not caused solely by a shift in ionization equilibrium. If we assume that multiple ionization is negligible compared to single ionization, we can use the Saha relation (Eq. (1)) to calculate number-density ratios between ionized and neutral states:

$$\frac{n_i + n_e}{n_0} = \frac{2}{\Lambda^3} \frac{g_i}{g_0} e\left(-\frac{\epsilon}{k_B T}\right) \quad (1)$$

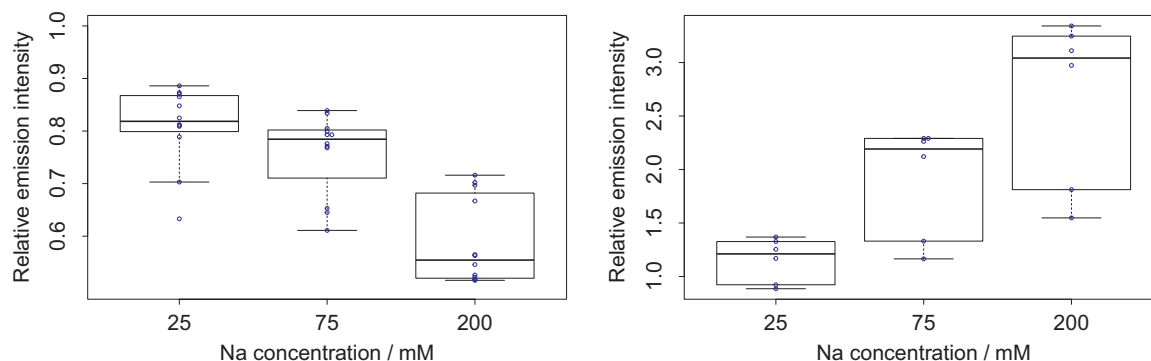


Fig. 2. Relative emission intensity for 18 analyte spectral lines (see Table 1 for line identities) at selected Na concentrations. Intensity in absence of Na has a value of unity. Left frame shows the Na matrix effect on ionic lines, right frame shows atomic lines. The bold black line represents the median of the data. Whiskers represent the quartiles with their ends being minimum and maximum of the collected data.

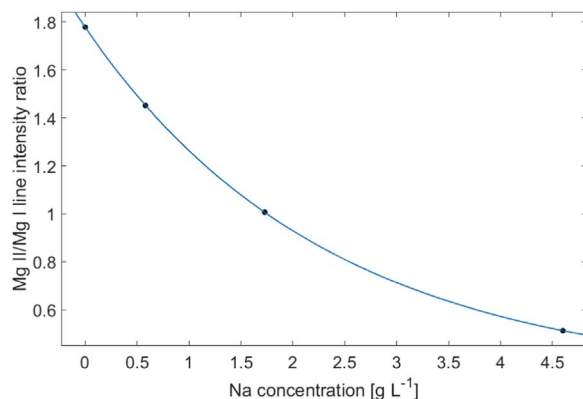


Fig. 3. Mg II 280.27 nm/Mg I 285.21 nm intensity ratio at selected Na concentrations. Mg concentration for all data points: $1 \mu\text{g mL}^{-1}$. Values are sum of signals over height in MICAP from 15 to 36 mm. Blue line shows the fit to an exponential decay: $y = a \cdot \exp(-b \cdot x) + c$; $a = 1.46$, $b = 0.433$, $c = 0.314$. (For interpretation of the references to color in this figure legend, the reader is referred to the web version of this article.).

where

n_e is electron number density, n_i the number density of species in the singly ionized state, n_o the number density of neutral species, λ the DeBroglie wavelength of an electron, g_i the degeneracy of states for the singly ionized state, g_o the degeneracy of states for the neutral species, ϵ the ionization energy, k_B the Boltzmann constant and T the ionization temperature.

From the Saha equation, any perturbation to the electron number density will cause a linear change in atom-ion equilibrium, which should also produce a linear decline in the Mg II/Mg I ratio as e^- number density goes up. However, any effect that lowers the ionization temperature (approximated by either electron or excitation temperature) will cause an exponential drop in the Mg II/Mg I ratio. Accordingly, a reduced ionization temperature could explain the trend in Fig. 3.

3.3. Sodium matrix effect at different analyte-element concentrations

At a Na matrix concentration of 75 mM, the fractional suppression of Mg II 279.55 nm emission is $\sim 34\%$, independent of the Mg concentration (cf. Fig. 4). The same behavior is observed for other Mg ion lines. This observation rules out a self-suppression of Mg II emission by Mg itself.

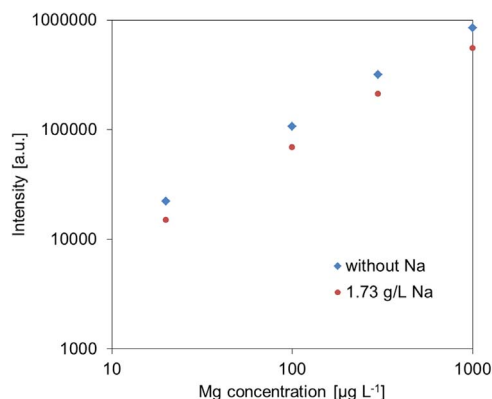


Fig. 4. Mg II 279.55 nm emission signal at different Mg concentrations without matrix (blue) and with 1.73 g L^{-1} (75 mM) Na (red) matrix. Note logarithmic scale. Values are sum of signals over height in MICAP from 15 to 36 mm. (For interpretation of the references to color in this figure legend, the reader is referred to the web version of this article.).

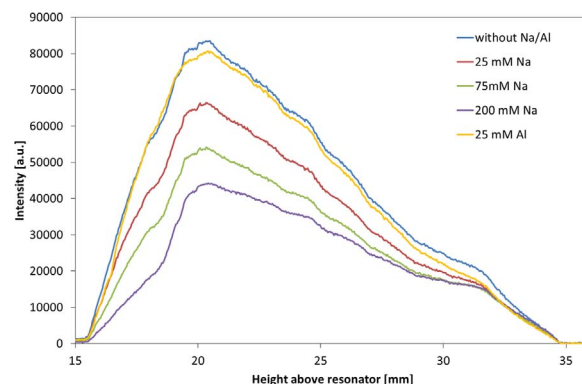


Fig. 5. Vertical spatial profile for Mg II 279.55 nm emission in the presence of Al and various Na concentrations.

3.4. Effect of sodium and aluminum matrices on spatial distribution of emitting species

In an Ar-ICP, the vertical distribution of elemental emission changes with instrumental parameters, overall sample composition, and plasma temperature [39–41]. The MICAP exhibits no similar matrix-dependent spatial shifts; examples are shown for Na and Al interference in Fig. 5 for Mg II emission and in Fig. 6 for Li I emission. For Mg II emission (Fig. 5), the shape of the vertical profiles remains the same at all examined sodium concentrations; only the intensity changes, with greater signal suppression occurring for higher Na concentrations. The effect of Al is similar to that of Na, but less pronounced, probably because of the higher ionization energy of Al. In contrast, for some neutral-atom lines, such as Li I 670.79 nm (Fig. 6), the emission is more uniformly distributed in the plasma, and with a Na-dependent signal enhancement. This behavior is in contrast to the radiation zones described for argon ICP-AES [40].

3.5. Effect of Na on Fe excitation temperature

If the effect of Na on the emission of other elements involves both a shift in ionization equilibrium and a drop in ionization temperature, there should be an influence of Na concentration on other temperatures in the MICAP as well. The excitation temperature, as a surrogate for ionization temperature, was measured by developing a Boltzmann plot, with Fe as the thermometric species. Ten Fe I lines with strong emission in the wavelength range of 360–380 nm were chosen. The corresponding gA values were taken from the NIST atomic spectra database [42]. With increasing Na concentration, the excitation temperature appeared to rise slightly first, to a maximum of 5300 K at a Na

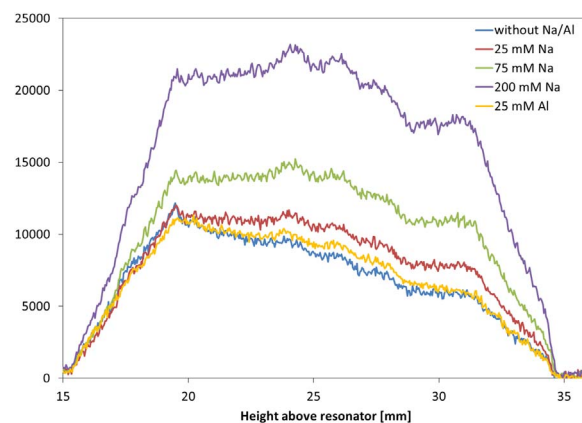


Fig. 6. Vertical spatial profile for Li I 670.79 nm emission in the presence of Al and various Na concentrations.

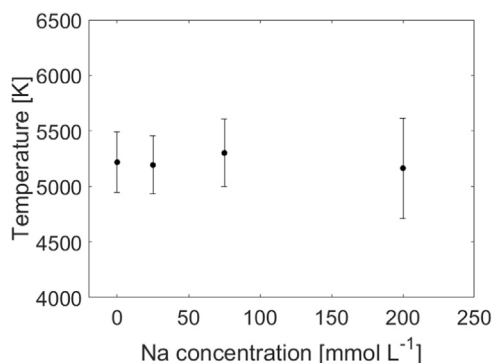


Fig. 7. Effect of Na concentration on the excitation temperature of the MICAP calculated from ten Fe I emission lines. Error bars represent deviation of linearity in the Boltzmann plot.

concentration of 75 mM, before declining at higher Na concentrations. The temperature returned to 5100 K at a Na concentration of 200 mM (cf. Fig. 7). Zhang et al. found for a nitrogen plasma in an Okamoto cavity a drop in excitation temperature of approximately 5% for 217 mM Na matrix [27]. However, the temperature drop was observed only at low microwave power and found to be negligible at 1.3 kW. Of course, temperature determination via the Boltzmann method is subject to high uncertainties (cf. error bars in Fig. 7). Accordingly, these data can only indicate a trend; still, the absence of an observable drop in Fe excitation temperature at a Na concentration of 75 mM (1.73 g L^{-1}) calls into question the hypothesis used earlier to explain the exponential decline in the Mg II/Mg I emission ratio seen in Fig. 3. Overall, the values here are similar to those of 5400–5500 K reported for other high-power nitrogen MIPs [38,43] but more than 1000 K below excitation temperatures in the Ar-ICP [44].

3.6. Methods for correcting matrix interference

There are several methods to overcome matrix interferences in emission spectrometry. In our preliminary experiments, Ca was tested as internal standard for Mg emission under the influence of a Na matrix. However, the Ca ion lines (396.8 and 393.4 nm) were suppressed differently from the Mg ionic lines; hence, the two do not constitute a useful internal standard pair. Internal standardization based on emission lines with excitation and ionization energies similar to the analyte element might be more successful.

Al-Ammar and Barnes proposed in 1998 a correction method for ICP-AES based on the evaluation of several emission lines of the same analyte element [45]. Two emission lines of the same element (e.g. Mg II 279.55 nm and Mg I 285.21 nm) exhibit significantly different relative emission intensities, so a correction factor can be calculated. A prerequisite for the use of this method is the existence of a well-defined trend of intensity versus matrix concentration. As described by Thompson et al. for a Ca matrix in ICP-AES, an exponential decay curve of the form

$$I = I_0 + A(1 - \exp(-Bc)) \quad (2)$$

can be fitted to the intensities at different matrix concentrations [46]. I is the measured intensity of the emission line, c the matrix concentration and A and B are adjustable parameters. Eq. (2) can also be applied here. An example is shown in Fig. 8 for the Mg II 279.55 nm emission line.

Based on this curve, a corrected signal for Mg II 279.55 nm emission can be calculated from the intensity ratio of the Mg II 279.55 nm to Mg I 285.21 nm lines. Al-Ammar's correction method was applied here. The method is in detail described elsewhere [45]; here the most important steps to obtain the results in Table 2 are listed:

1. The Mg II 279.55 emission line is chosen as an analyte line I_a ; the Mg

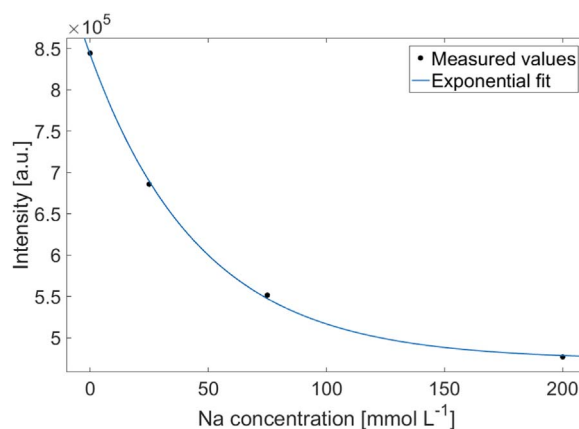


Fig. 8. Measured intensity I of Mg II 279.55 nm emission line vs. Na concentration c with data fitted to an exponential decay $I = I_0 + A(1 - \exp(-Bc))$.

Table 2

Matrix-effect correction using spectral lines of the same analyte as internal standard.

Expected	Found uncorrected	Found corrected
100 ppb	48.5 ppb	91.8 ppb
300 ppb	221.8 ppb	354.1 ppb
1000 ppb	632.4 ppb	988.2 ppb

1. 285.21 nm emission line is chosen as a reference line I_b .

2. The ratio of analyte line intensity to analyte line intensity at different matrix concentrations I_a^0/I_a is calculated.
3. The ratio of analyte line intensity to reference line intensity I_a/I_b at different matrix concentrations is calculated.
4. I_a^0/I_a is plotted against I_a/I_b and the slope and intercept of the straight line is determined.
5. Now the intensity of the two Mg emission lines is measured for an unknown matrix concentration. The line intensity ratio I_a/I_b is determined.
6. Based on the straight-line equation determined previously (step 4) the ratio I_a^0/I_a is calculated for the measured intensities at unknown matrix concentration.
7. The resulting correction factor is multiplied by the measured intensity of the analyte line. This corrected intensity can now be used to determine the corrected concentration based on the calibration curve obtained in laboratory without matrix constituents.

Table 2 shows the result for three Mg concentrations. The data indicate the efficacy of this method for matrix correction.

One of the most effective methods to reduce matrix effects in argon ICP-AES is to reduce the sample injector flow or to enlarge the injector tube [47–49]. Both methods increase the residence time of the aerosol in the plasma, leading to a larger zone of energy exchange between the central channel and the surrounding plasma [48]. Additionally, a reduction in the carrier-gas flow-rate produces an increase in plasma temperature [50]. In the present work, the central-channel flow was reduced from 1 L min^{-1} to 0.54 L min^{-1} . Fig. 9 compares the relative emission intensities for the three investigated Mg emission lines (both neutral atom and ion) at several matrix concentrations. It demonstrates that the ion-signal suppression shows less dependence on Na concentration at the lower flow rate; i.e. relative emission intensities are closer to 1. A complete removal of the matrix effect was not found to be possible; in addition, a lower central flow rate led to a four-fold signal reduction, thus raising also the detection limit.

4. Conclusion

The matrix effect of Na at several concentrations on 18 emission

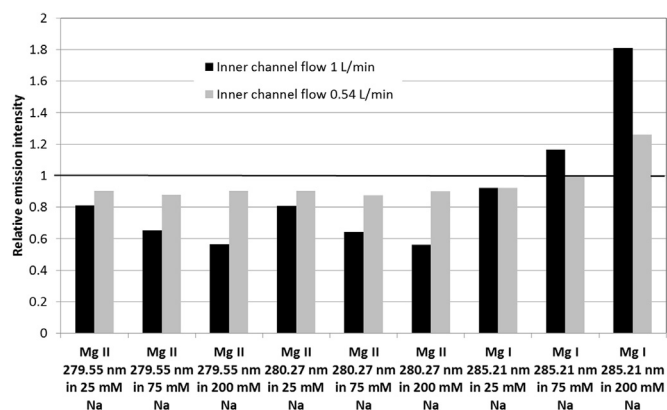


Fig. 9. Effect of reduced central-channel flow on relative emission intensities of Mg transitions at several Na matrix concentrations.

lines of 8 elements has been investigated. A suppression of ionic lines and an enhancement of atomic lines was observed that became stronger at increasing Na concentrations. Similar but less pronounced behavior was found for Al. The Na or Al matrix effect has no significant influence on the shape of the vertical spatial emission profiles for the investigated spectral lines, different from what has been observed in argon ICP-AES. The observations could be explained by a matrix effect that causes both a shift in ionization equilibrium and a change in ionization temperature. However, the excitation temperature of the plasma, used to approximate the ionization temperature, was determined by the Boltzmann plot method from Fe I lines at selected Na concentrations. The excitation temperature changes only slightly, with variations being less than 10% for a range of matrix concentrations. It must therefore be determined whether the excitation temperature in the MICAP correlates well with the ionization temperature.

Measurement of Thomson scattering would give spatially resolved information on electron densities, electron temperatures and gas-kinetic temperatures [51,52]. Such a study would be valuable to complete our understanding of matrix-based emission interferences in the MICAP. Correction methods to minimize the matrix interferences have been briefly evaluated here but further work is needed. For example, the addition of hydrogen to the plasma might help serve as a buffer to reduce the matrix effect [53]. These additional studies are needed for a more complete characterization of the interferences and to develop methods to mitigate matrix effects in the MICAP.

Acknowledgments

The authors are grateful to Radom for providing the MICAP used in this study and to Meinhard Associates for donation of the ICP torches and nebulizer. This work was supported by the U.S. Department of Energy through grant DOE DE-FG02-98ER 14890 and by the Deutsche Forschungsgemeinschaft (DFG) through the TUM International Graduate School of Science and Engineering (IGSSE).

References

- [1] P.W.J.M. Boumans, *Inductively Coupled Plasma Emission Spectroscopy*, Wiley, New York, 1987.
- [2] S. Becker, *Inorganic Mass Spectrometry: Principles and Applications*, Wiley, 2008.
- [3] J.M. Keane, R.C. Fry, Red and near-infrared inductively coupled plasma emission spectra of fluorine, chlorine, bromine, iodine, and sulfur with a photodiode array detector, *Anal. Chem.* 58 (4) (1986) 790–797.
- [4] A.L. Gray, Mass-spectrometry with an inductively coupled plasma as an ion-source – the influence on ultratrace analysis of background and matrix response, *Spectrochim. Acta B* 41 (1–2) (1986) 151–167.
- [5] S.H. Tan, G. Horlick, Background spectral features in inductively coupled plasma mass-spectrometry, *Appl. Spectrosc.* 40 (4) (1986) 445–460.
- [6] J.S. Becker, H.J. Dietze, Double-focusing sector field inductively coupled plasma mass spectrometry for highly sensitive multi-element and isotopic analysis - Invited lecture, *J. Anal. At. Spectrom.* 12 (9) (1997) 881–889.

- [7] I. Feldmann, N. Jakubowski, D. Stuewer, Application of a hexapole collision and reaction cell in ICP-MS Part I: instrumental aspects and operational optimization, *Fresenius' J. Anal. Chem.* 365 (5) (1999) 415–421.
- [8] J. Hubert, M. Moisan, A. Ricard, New microwave plasma at atmospheric-pressure, *Spectrochim. Acta B* 34 (1) (1979) 1–10.
- [9] C.I.M. Beenakker, Cavity for microwave-induced plasmas operated in helium and argon at atmospheric-pressure, *Spectrochim. Acta B* 31 (8–9) (1976) 483–486.
- [10] C.I.M. Beenakker, Evaluation of a microwave-induced plasma in helium at atmospheric-pressure as an element-selective detector for gas-chromatography, *Spectrochim. Acta B* 32 (3–4) (1977) 173–187.
- [11] K. Tanabe, H. Haraguchi, K. Fuwa, Application of an atmospheric-pressure helium microwave-induced plasma as an element-selective detector for gas-chromatography, *Spectrochim. Acta B* 36 (7) (1981) 633–639.
- [12] Y. Okamoto, Annular-shaped microwave-induced nitrogen plasma at atmospheric-pressure for emission-spectrometry of solutions, *Anal. Sci.* 7 (2) (1991) 283–288.
- [13] M. Selby, G.M. Hieftje, Taming the surfatron, *Spectrochim. Acta B* 42 (1–2) (1987) 285–298.
- [14] R.D. Deutsch, G.M. Hieftje, Development of a microwave-induced nitrogen discharge at atmospheric-pressure (Mindap), *Appl. Spectrosc.* 39 (2) (1985) 214–222.
- [15] J.T. Creed, T.M. Davidson, W.L. Shen, P.G. Brown, J.A. Caruso, Helium microwave induced plasma mass-spectrometry for detection of metals and nonmetals in aqueous-solutions, *Spectrochim. Acta B* 44 (9) (1989) 909–924.
- [16] C.I.M. Beenakker, B. Bosman, P.W.J.M. Boumans, Assessment of a microwave-induced plasma generated in argon with a cylindrical Tm010 cavity as an excitation source for emission spectrometric analysis of solutions, *Spectrochim. Acta B* 33 (7) (1978) 373–381.
- [17] M.H. Abdallah, S. Coulombe, J.M. Mermet, J. Hubert, An assessment of an atmospheric-pressure helium microwave plasma produced by a surfatron as an excitation source in atomic emission-spectroscopy, *Spectrochim. Acta B* 37 (7) (1982) 583–592.
- [18] Q.H. Jin, C. Zhu, M.W. Borer, G.M. Hieftje, A microwave plasma torch assembly for atomic emission-spectrometry, *Spectrochim. Acta B* 46 (3) (1991) 417–430.
- [19] Y. Okamoto, High-sensitivity microwave-induced plasma mass spectrometry for trace element analysis, *J. Anal. At. Spectrom.* 9 (7) (1994) 745–749.
- [20] K. Oishi, T. Okumoto, T. Iino, M. Koga, T. Shirasaki, N. Furuta, Elemental mass spectrometry using a nitrogen microwave-induced plasma as an ion source, *Spectrochim. Acta Part B: At. Spectrosc.* 49 (9) (1994) 901–914.
- [21] K. Jankowski, E. Reszke, Recent developments in instrumentation of microwave plasma sources for optical emission and mass spectrometry: tutorial review, *J. Anal. At. Spectrom.* 28 (8) (2013) 1196–1212.
- [22] K. Jankowski, Microwave induced plasma emission spectrometry for environmental analysis. A review, *Chem. Anal.-Wars.* 46 (3) (2001) 305–327.
- [23] H. Takahara, M. Iwasaki, Y. Tanibata, Particle analyzer system based on microwave-induced plasma technology, *IEEE Trans. Instrum. Meas.* 44 (3) (1995) 819–823.
- [24] Y.X. Duan, Y.X. Su, Z. Jin, S.P. Abeln, A field portable plasma source monitor for real-time air particulate monitoring, *Anal. Chem.* 72 (7) (2000) 1672–1679.
- [25] J.J. Urh, J.W. Carnahan, Analytical figures of merit and interelement effects with air and nitrogen microwave-induced plasmas, *Appl. Spectrosc.* 40 (6) (1986) 877–883.
- [26] J.L. Todoli, L. Gras, V. Hernandis, J. Mora, Elemental matrix effects in ICP-AES, *J. Anal. At. Spectrom.* 17 (2) (2002) 142–169.
- [27] Z.N. Zhang, K. Wagatsuma, Matrix effects of easily ionizable elements and nitric acid in high-power microwave-induced nitrogen plasma atomic emission spectrometry, *Spectrochim. Acta B* 57 (8) (2002) 1247–1257.
- [28] J.P. Matousek, B.J. Orr, M. Selby, Interferences due to easily ionized elements in a microwave-induced plasma system with graphite-furnace sample introduction, *Spectrochim. Acta B* 41 (5) (1986) 415–429.
- [29] H.R. Griem, Principles of plasma spectroscopy, in: J.E. Thompson, L.H. Luessen (Eds.), *Fast Electrical and Optical Measurements: Volume I — Current and Voltage Measurements / Volume II — Optical Measurements*, Springer, Netherlands, Dordrecht, 1986, pp. 885–910.
- [30] A.J. Schwartz, Y. Cheung, J. Jevtic, V. Pikelja, A. Menon, S.J. Ray, G.M. Hieftje, New inductively coupled plasma for atomic spectrometry: the microwave-sustained, inductively coupled, atmospheric-pressure plasma (MICAP), *J. Anal. At. Spectrom.* 31 (2) (2016) 440–449.
- [31] G.R. Kornblum, L. De Galan, Ionization interference in the acetylene-nitrous oxide flame, *Spectrochim. Acta Part B: At. Spectrosc.* 28 (4) (1973) 139–147.
- [32] E.E. Pickett, S.R. Koirtiyohann, Nitrous oxide-acetylene flame in emission analysis. I. General characteristics, *Spectrochim. Acta B* 23 (4) (1968) 235.
- [33] M.W. Blades, G. Horlick, Interference from easily ionizable element matrices in inductively coupled plasma emission-spectrometry – a spatial study, *Spectrochim. Acta B* 36 (9) (1981) 881–900.
- [34] A. Kramida, Y. Ralchenko, J. Reader, N.A.T. NIST Atomic Spectra Database (ver. 5.2) [Online], National Institute of Standards and Technology, Gaithersburg, MD, 2014, p. 2014 <https://physics.nist.gov/asd>.
- [35] J.M. Mermet, Use of magnesium as a test element for inductively coupled plasma atomic emission-spectrometry diagnostics, *Anal. Chim. Acta* 250 (1) (1991) 85–94.
- [36] J.-M. Mermet, E. Poussel, ICP emission spectrometers: 1995 analytical figures of merit, *Appl. Spectrosc.* 49 (10) (1995) 12A–18A.
- [37] D.A. Goncalves, T. McSweeney, G.L. Donati, Characteristics of a resonant iris microwave-induced nitrogen plasma, *J. Anal. At. Spectrom.* 31 (5) (2016) 1097–1104.
- [38] M. Ohata, N. Furuta, Spatial characterization of emission intensities and temperatures of a high power nitrogen microwave-induced plasma, *J. Anal. At. Spectrom.* 12 (3) (1997) 341–347.
- [39] M.W. Blades, G. Horlick, The vertical spatial characteristics of analyte emission in

- the inductively coupled plasma, *Spectrochim. Acta B* 36 (9) (1981) 861–880.
- [40] S.R. Koirtyohann, J. Stephen Jones, C.P. Jester, D.A. Yates, Use of spatial emission profiles and a nomenclature system as aids in interpreting matrix effects in the low-power argon inductively coupled plasma, *Spectrochim. Acta Part B: At. Spectrosc.* 36 (1) (1981) 49–59.
- [41] R.N. Savage, G.M. Hieftje, Vaporization and ionization interferences in a miniature inductively coupled plasma, *Anal. Chem.* 52 (8) (1980) 1267–1272.
- [42] A. Kramida, Y. Ralchenko, J. Reader, N.A. Team, NIST Atomic Spectra Database (ver. 5.3) (Online), National Institute of Standards and Technology, Gaithersburg, MD, 2015.
- [43] K. Ogura, H. Yamada, Y. Sato, Y. Okamoto, Excitation temperature in high-power nitrogen microwave-induced plasma at atmospheric pressure, *Appl. Spectrosc.* 51 (10) (1997) 1496–1499.
- [44] N. Furuta, Spatial profile measurement of ionization and excitation temperatures in an inductively coupled plasma, *Spectrochim. Acta B* 40 (8) (1985) 1013–1022.
- [45] A.S. Al-Ammar, R.M. Barnes, Correction for non-spectroscopic matrix effects in inductively coupled plasma-atomic emission spectroscopy by internal standardization using spectral lines of the same analyte, *Spectrochim. Acta B* 53 (11) (1998) 1583–1593.
- [46] M. Thompson, M.H. Ramsey, Matrix effects due to calcium in inductively coupled plasma atomic-emission spectrometry – their nature, source and remedy, *Analyst* 110 (12) (1985) 1413–1422.
- [47] R. Rezaaiyaan, G.M. Hieftje, Analytical characteristics of a low-flow, low-power inductively coupled plasma, *Anal. Chem.* 57 (2) (1985) 412–415.
- [48] J.M. Mermet, Ionic to atomic line intensity ratio and residence time in inductively coupled plasma atomic emission-spectrometry, *Spectrochim. Acta B* 44 (11) (1989) 1109–1116.
- [49] C. Dubuisson, E. Poussel, J.M. Mermet, Comparison of axially and radially viewed inductively coupled plasma atomic emission spectrometry in terms of signal-to-background ratio and matrix effects – plenary lecture, *J. Anal. At. Spectrom.* 12 (3) (1997) 281–286.
- [50] M. Marichy, M. Mermet, M. Murillo, E. Poussel, J.-M. Mermet, Detection limit scale in inductively coupled plasma atomic emission spectrometry, *J. Anal. At. Spectrom.* 4 (2) (1989) 209–212.
- [51] D.S. Hanselman, N.N. Ses, M. Huang, G.M. Hieftje, The effect of sample matrix on electron density, electron temperature and gas temperature in the argon inductively coupled plasma examined by Thomson and Rayleigh scattering, *Spectrochim. Acta Part B: At. Spectrosc.* 49 (5) (1994) 495–526.
- [52] N. Chalyavi, P.S. Doidge, R.J.S. Morrison, G.B. Partridge, Fundamental studies of an atmospheric-pressure microwave plasma sustained in nitrogen for atomic emission spectrometry, *J. Anal. At. Spectrom.* 32 (10) (2017) 1988–2002.
- [53] I. Novotny, J.C. Farinas, J.L. Wan, E. Poussel, J.M. Mermet, Effect of power and carrier gas flow rate on the tolerance to water loading in inductively coupled plasma atomic emission spectrometry, *Spectrochim. Acta B* 51 (12) (1996) 1517–1526.